Available online at www.sciencedirect.com

ScienceDirect

journal homepage: www.elsevier.com/locate/he

In situ X-ray CT visualization of hydrogen bubbles inside the porous transport layer of a direct toluene electro-hydrogenation electrolyzer

Fátima I. Reyna-Peña [a,*], *Antonio Atienza-Márquez* [b,c], *Sunpil Jang* [a], *Ryuhei Shiono* [a], *Kaito Shigemasa* [a], *Takuto Araki* [e], *Kensaku Nagasawa* [d], *Shigenori Mitsushima* [c,f]

[a] *Yokohama National University, Graduate School of Engineering Science, Tokiwadai 79-5, Hodogaya-ku, Yokohama, 240-8501, Japan*

[b] *Universitat Rovira I Virgili, Mechanical Engineering Department, Group of Applied Thermal Engineering (CREVER), Av. Països Catalans 26, 43007 Tarragona, Spain*

[c] *Yokohama National University, Institute of Advanced Sciences (IAS), Tokiwadai 79-5, Hodogaya-ku, Yokohama, 240-8501, Japan*

[d] *National Institute of Advanced Industrial Science and Technology (AIST), Fukushima Renewable Energy Institute, 2-2-9 Machiikedai, Koriyama, Fukushima 963-0298, Japan*

[e] *Yokohama National University, Faculty of Engineering, Division of Systems Research, 79-5, Hodogaya-ku, Yokohama, 240-8501, Japan*

[f] *Yokohama National University, Green Hydrogen Research Center, 79-5, Hodogaya-ku, Yokohama, 240-8501, Japan*

HIGHLIGHTS

- Direct toluene electro-hydrogenation electrolyzer for efficient hydrogen transport.
- Hydrogen bubbles generated from side reaction inhibit toluene mass transport.
- First in situ X-ray visualization of hydrogen bubbles inside the porous electrode.
- More hydrogen bubbles observed at higher current densities and after longer operation.
- Ribbed flow field plates could reduce the hydrogen bubbles inside a porous electrode.

GRAPHICAL ABSTRACT

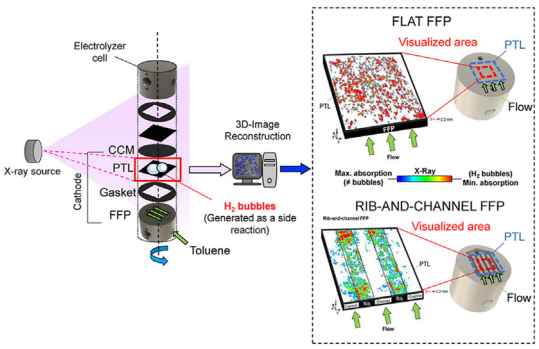

ARTICLE INFO

Article history:
Received 7 June 2023

ABSTRACT

The organic hydride toluene/methylcyclohexane is an attractive hydrogen carrier. The direct electro-hydrogenation of toluene to methylcyclohexane has a higher energy efficiency

* *Corresponding author.*
E-mail address: reyna-isabella-yd@ynu.jp (F.I. Reyna-Peña).

https://doi.org/10.1016/j.ijhydene.2023.08.132

Please cite this article as: Reyna-Peña FI et al., In situ X-ray CT visualization of hydrogen bubbles inside the porous transport layer of a direct toluene electro-hydrogenation electrolyzer, International Journal of Hydrogen Energy, https://doi.org/10.1016/j.ijhydene.2023.08.132

Received in revised form
7 August 2023
Accepted 9 August 2023
Available online xxx

Keywords:
Direct toluene electro-hydrogenation
Hydrogen
Bubbles visualization
Porous transport layer
X-ray CT
PEM electrolyzer

compared to the conventional two-step method. Yet, there are factors inhibiting the toluene supply to the cathode reaction site and reducing the conversion rate to methylcyclohexane. Thus, hydrogen may be generated as a side reaction. Understanding how hydrogen bubbles are distributed is crucial regarding the design optimization of these electrochemical devices. This work presents, for the first time in a direct toluene electro-hydrogenation electrolyzer, the X-ray visualization of hydrogen bubbles inside the porous electrode. The concentration of bubbles was higher near the cathode catalyst and tended to increase with the electric current and operating time. Bubble distribution spreads across the active area when using flat field plates. As for rib-and-channel field plates, despite bubbles mostly concentrated beneath ribs, the total hydrogen accumulated inside the porous electrode could be reduced.

1. Introduction

A greater share of renewable energies is central to curving the carbon footprint of the current energy mix and limiting the global temperature rise [1]. However, the transition towards a net-zero energy system cannot be addressed overnight [2], and the current energy crisis hinders the deployment of sustainable energy ecosystems [3]. Year over year greenhouse gas (GHG) emissions continue to grow because of the unabated use of pollutant fossil fuels [4]. Besides, renewables (e.g., solar or wind) face bottlenecks derived from their unequal geographical distribution or intermittent nature. Therefore, there are locations where the use of green electricity through direct electrification is technically unfeasible; energy storage and transport technologies are usually required.

Green hydrogen (herein H_2), produced via water electrolysis, is an attractive energy vector concerning long-haul transport and seasonal storage of green electricity [5]. Nevertheless, the exceptionally low volumetric energy density of H_2 complicates its storage (*e.g.*, 0.003 kWh/L-H_2 versus 8.6 kWh/L-gasoline [6]). Among the variety of hydrogen storage solutions (e.g., compressed, and liquefied H_2, metal hydrides, and so forth [7]), liquid organic hydrogen carriers (LOHCs) are one of the most promising. Most LOHCs are in the liquid phase at ambient temperature and pressure, which may enable using the existing oil infrastructure. LOHCs are based on reversible hydrogenation and de-hydrogenation cycles and, unlike circular H_2 carriers (*e.g.*, ammonia, formic acid, or methanol [8]), without binding or releasing other substances to/from the atmosphere [9].

There are numerous LOHCs candidates [10]; yet none of them is ideal in terms of storage capacity, energy density, temperature range at liquid state, de-hydrogenation heat and temperature, de-hydrogenation indicators (i.e., amount of heat, temperature, and rate of H_2 release), safety, availability, or cost. For instance, the naphthalene/decalin system has good storage capacity (*i.e.*, 7.3 wt% and 2.2 kWh/L), but its high toxicity and solid state at ambient temperature are issues [11]. Benzene/cyclohexane also exhibits high H_2 content, but benzene is a carcinogen [12]. Toluene/methylcyclohexane (MCH) needs elevated temperatures for de-hydrogenation, and its volumetric energy density (*i.e.*, ≈1.6 kWh/L) is lower than that of other hydrogen carriers such as liquid H_2 or ammonia [13]. Nonetheless, this organic hydride system is an easily manageable and stable liquid over a wide temperature range (i.e., between 162-384 K and 146−374 K for toluene and MCH, respectively [6]). In addition, it has low toxicity, exhibits gasoline-like features, and has been identified as the most cost-effective technology for the large-scale overseas transportation of hydrogen [14].

The conventional hydrogenation of toluene to MCH consists of a two-step process. First, H_2 is produced. Subsequently, H_2 is added to toluene through the following exothermic reaction [15]:

$$C_6H_5CH_3 + 3H_2 \rightarrow C_6H_{11}CH_3, \qquad \Delta H = -205\ \mathrm{kJ/mol} \tag{1}$$

As a promising alternative, the direct toluene hydrogenation technology relies on a single-step process using proton exchange membrane (PEM) electrolyzers (Fig. 1) and avoids the associated thermal losses. Besides, the theoretical voltage of toluene direct electro-hydrogenation is lower than that of electrochemical water splitting (i.e., 1.08 V versus 1.23 V, respectively). Hence, the electric power consumption may be lower than that of the conventional toluene hydrogenation technique [16].

The basic operating principle of a direct toluene electro-hydrogenation electrolyzer is illustrated in Fig. 1. Water splitting occurs at the anode electrode. Protons migrate through the membrane and reach the cathode catalyst layer (CL), where they react with both the electrons transferred via the external circuit and the toluene transported through the porous transport layer (PTL). Thus, toluene is converted to MCH. The following reactions occur, simultaneously, at both electrodes [17]:

$$\mathrm{Anode}: 2\,H_2O \rightarrow O_2 + 4\,H^+ + 4\,e^- \tag{2.1}$$

$$\mathrm{Cathode}: C_7H_8 + 6H^+ + 6e^- \rightarrow C_7H_{14} \tag{2.2}$$

Yet in practice, the overall conversion ratio could be lower than 100%. The sufficient toluene supply to the cathode catalyst layer is a critical issue. It has been assumed that the toluene path to the reaction site is partially blocked by the water dragged from the anode side [18], as well as by the increase of MCH concentration. Consequently, hydrogen bubbles are generated as a side reaction at the cathode catalyst electrode (Fig. 1) [16]. Moreover, the H_2 bubbles may stay at the

Please cite this article as: Reyna-Peña FI et al., In situ X-ray CT visualization of hydrogen bubbles inside the porous transport layer of a direct toluene electro-hydrogenation electrolyzer, International Journal of Hydrogen Energy, https://doi.org/10.1016/j.ijhydene.2023.08.132

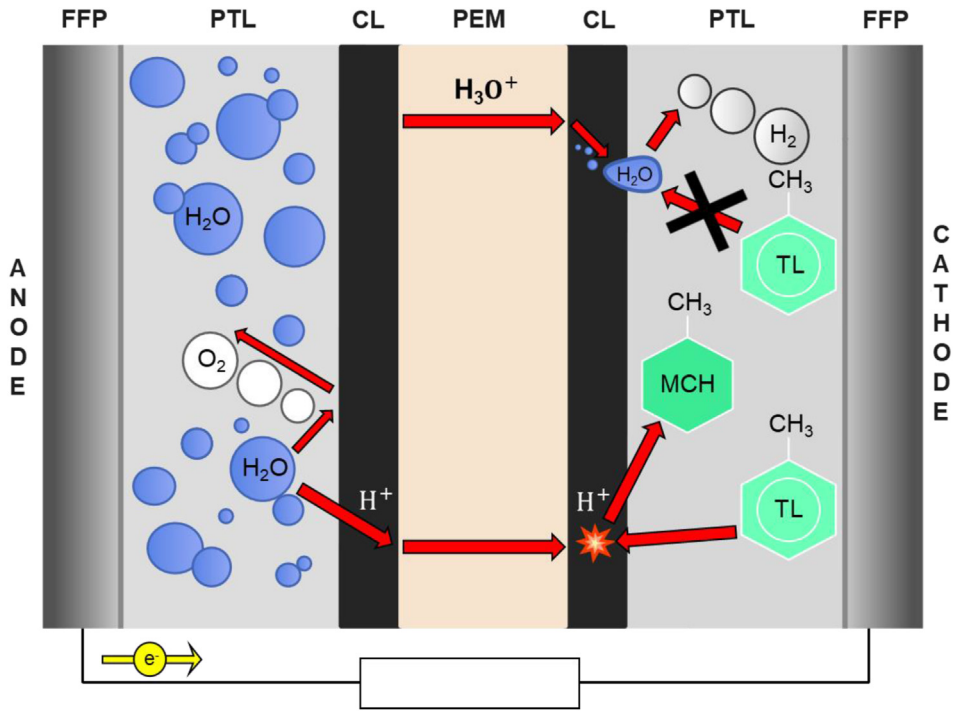

Fig. 1 – Schematic diagram of direct toluene electro-hydrogenation in a PEM-type electrolyzer of toluene flow affected by the H_2 bubble generation.

cathode catalyst layer and the PTL, thereby, further inhibiting the toluene mass transfer [19].

To improve the electrochemical performance, previous works have attempted to enhance the toluene mass transport under a "*trial and error*" approach. For example, Nagasawa et al. [20] investigated the effect of different cathode flow field structures on electrochemical performance. Also, it has been studied the effect of the operating temperature and the toluene concentration on the mass transfer limit at the cathode side [21]. It was determined that the use of materials with long side chain structure and high equivalent weight (e.g., Nafion™), for both the membrane and ionomer, better suppresses the hydrogen generation [22]. Besides, it was found that the use of a Pt-loaded carbon paper flow-field promotes the chemical-hydrogenation of toluene with the generated hydrogen bubbles [17], and the activity of the PtRu/C catalyst layer for the electro-hydrogenation of toluene was higher than that of Pt/C-coated catalyst [23]. Recently, it was found that an optimum thickness of the cathode catalyst layer corresponding to catalyst loadings of 1.4–1.6 mg/cm^2 could maximize the current efficiency of the electrolyzer [19].

Visualization studies shed light on the mass transfer phenomena in electrochemical devices [24]. Shigemasa et al. [16] showed the visualization of both water droplets and generated H_2 bubbles on the surface of the cathode's PTL using a high-speed camera. Nevertheless, there is a research gap on how bubbles are distributed near the reaction site and across the PTL in toluene direct electro-hydrogenation cells.

X-ray imaging techniques provide non-invasive optical access to the processes occurring inside electrochemical cells [25]. Indeed, X-rays are widely used in numerous studies dealing with hydrogen technologies, for example, for the in situ visualization of liquid water inside operating PEM fuel cells [26,27], or oxygen bubbles in PEM water electrolyzers [28,29]. For instance, Markötter et al. [30] performed a study of water distribution in a PEM fuel cell with a perforated gas diffusion layer at the cathode side. Kato et al. [31] also used X-ray to quantify the cross-flow rate and the amount of liquid water in gas diffusion layers with different thicknesses. On the other hand, despite many studies that have been developed using synchrotron facilities [32], micro X-ray computed tomography (CT) allows gaining detailed insight into the porous electrode [33] with lower cost and major availability [34].

The aim of this paper is the in situ X-ray CT visualization, for the very first time, of hydrogen bubbles inside the cathode PTL of a direct toluene electro-hydrogenation electrolyzer. To accomplish the objective, an in-house cell was developed, and various scenarios were considered in terms of flow fields, electric current density, and operating time. This will provide worthy information to optimize the design and concerning middle-term development of this electrochemical technology.

The structure of the paper is as follows. After the introduction and objective, Section 2 describes the experimental setup and conditions. Afterward, Section 3 presents the discussion of the visualization results obtained. Finally, the main conclusions are summarized in Section 4.

2. Experimental

2.1. *Cell configuration and components*

Fig. 2 shows the experimental setup and the developed in-house electrochemical cell used in this research. It consists

Please cite this article as: Reyna-Peña FI et al., In situ X-ray CT visualization of hydrogen bubbles inside the porous transport layer of a direct toluene electro-hydrogenation electrolyzer, International Journal of Hydrogen Energy, https://doi.org/10.1016/j.ijhydene.2023.08.132

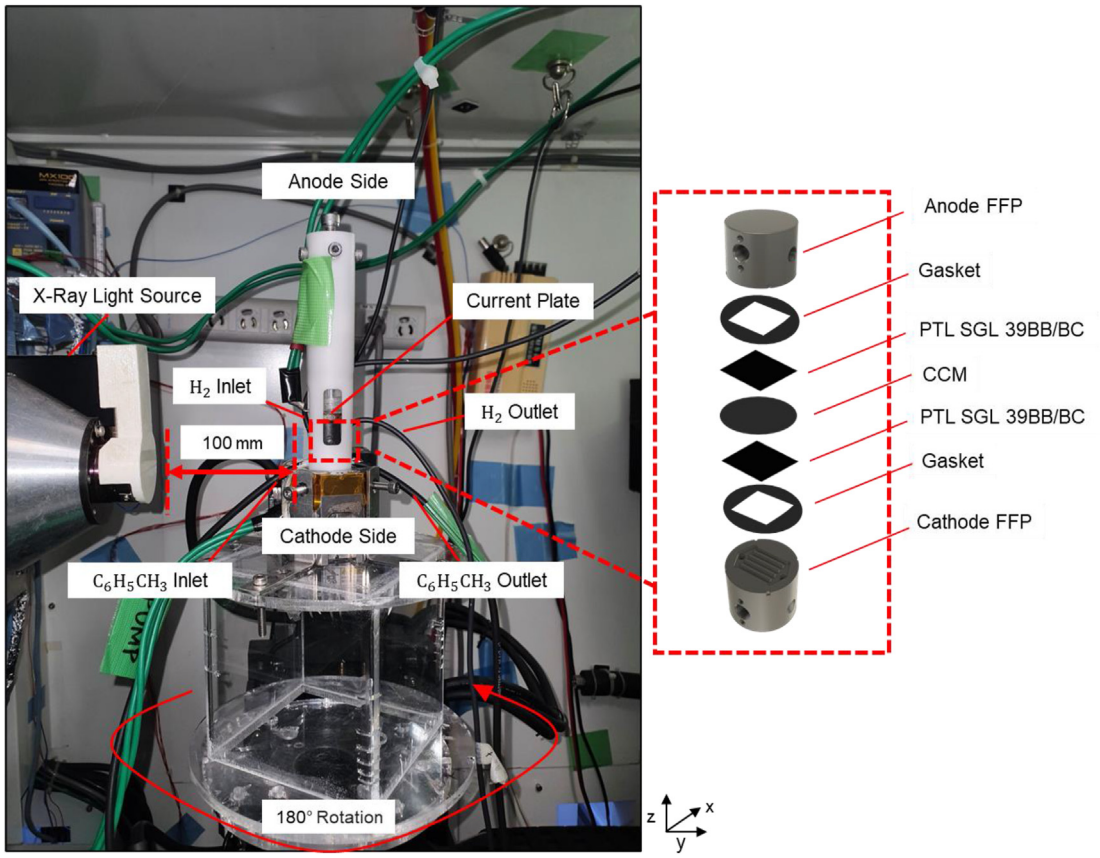

Fig. 2 – Image of the electrolyzer cell inside the X-Ray CT-Scan system.

of a vertical sandwich-like configuration, integrated by a gasket (cathode side), cathode-porous transport layer (PTL), catalyst-coated membrane (CCM), anode-PTL, and gasket (anode side). These components are clamped between the flow field plates (FFPs).

This cell was engineered to investigate, through visualization experiments, the distribution of hydrogen bubbles inside the cathode PTL. To enable visualizations within the cell, an acrylic enclosure (Fig. 2) was utilized to provide support and hold the components securely in place. The supply of the fluid reactants for both the anode and cathode were located at the top and bottom of the cell, respectively. The X-ray CT scan captured images while the cell rotated, with its vertical alignment at the middle center of the cell. This positioning allowed for visualizations inside the cathode PTL.

Unlike conventional PEM electrolyzers that use water as an electrolyte [35], in this study, the anode is supplied with hydrogen gas, while the cathode is supplied with toluene. The reason behind this choice is to investigate the distribution of gas bubbles, which is a crucial factor affecting the performance of direct toluene electro-hydrogenation electrolyzers. By focusing on the hydrogen supply, we aim to gain insights into the behavior of gas bubbles inside the PTL and their impact on the efficiency of the system.

To analyze the effect of the toluene supply flow field on the hydrogen bubble's mass transport and distribution pattern inside the cathode PTL, the following two FFP geometries were considered: flat and rib-and-channel. Fig. 3 shows a three-dimensional (3D) view of both FFPs and their flow field distributions. The diagram illustrates the specific patterns and directions of fluid flow within each FFP, allowing a better understanding of the flow dynamics and how they differ between the two FFPs [36]. The flat FFP serves as a reference point to assess the cell's performance without any specific flow channel structure. On the other hand, we are also examining the rib-and-channel structure, which induces a parallel flow pattern widely used in conventional PEM-type electrolyzers and fuel cells [37]. The material used for the FFPs was graphite G347B (Tokai Carbon Co., Ltd. [38]) with excellent electrical and terminal conductivity, and whose molecular weight is like that of toluene, thereby enabling flow visualization using X-ray technology.

The CCM was cropped to a 20 mm-diameter circular shape (Fig. 2) for the sake of better cell assembling, to prevent cross-leakage and ensure a more effective conversion. The electrolyte thickness was ≈12 μm (GORE-SELECT® [39]) and the catalyst was placed in the middle center of the FFP with a reaction area of 1 cm^2.

As for the PTLs, Sigracet 39 series non-woven carbon fiber paper with a Microporous Layer (MPL) that has been PTFE treated to 5% and 80% porosity [40]. Type 39BC (325 μm-thick, <12 mΩ cm^2 through-plane electrical resistivity) was used, both at the anode and cathode sides, for those experiments using the flat FFP. The manufacturer permanently replaced the 39BC type with 39BB (315 μm-thick, <13 mΩ cm^2 through-plane electrical resistivity), which was the PTL used for the

Please cite this article as: Reyna-Peña FI et al., In situ X-ray CT visualization of hydrogen bubbles inside the porous transport layer of a direct toluene electro-hydrogenation electrolyzer, International Journal of Hydrogen Energy, https://doi.org/10.1016/j.ijhydene.2023.08.132

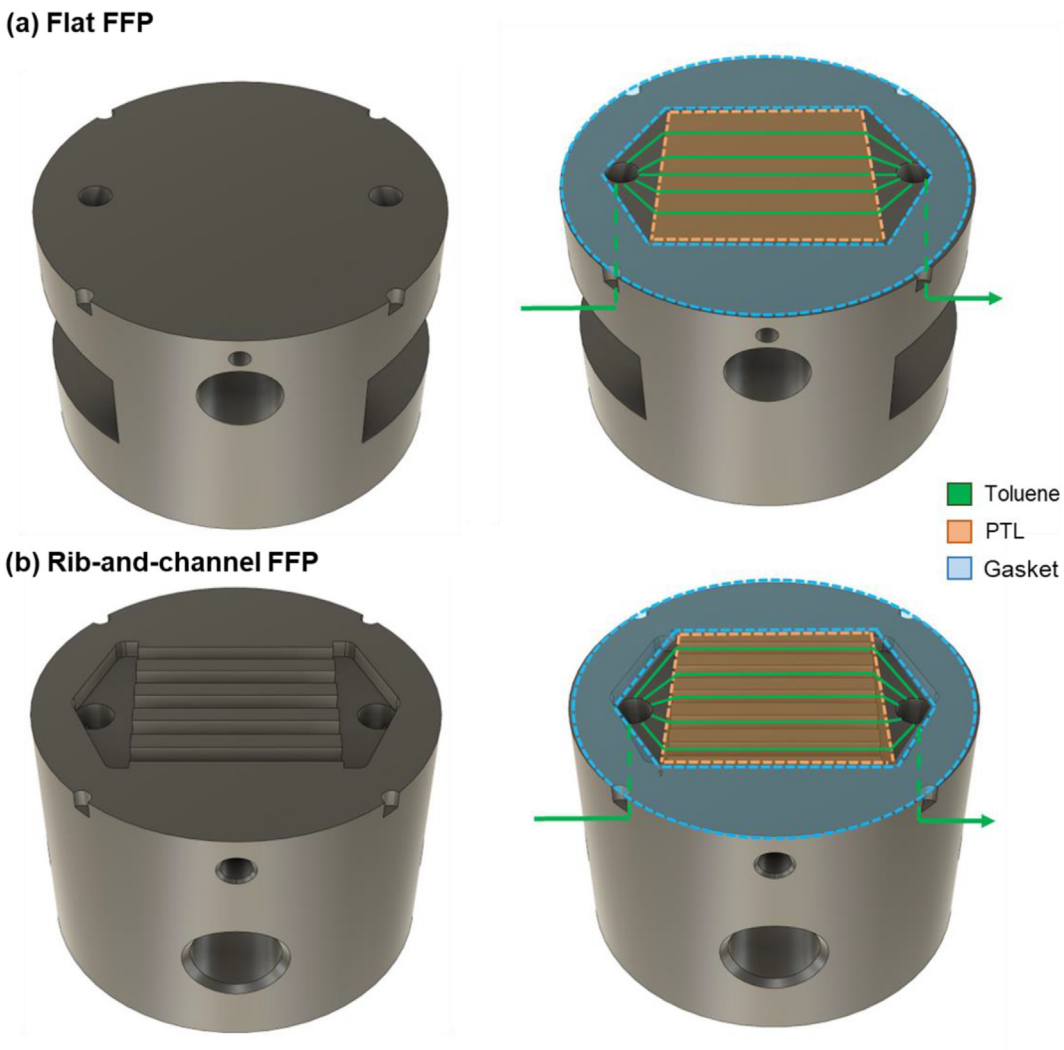

Fig. 3 – Flow field plate geometries considered: (a) Flat and (b) Rib-and-channel.

experiments using the ribbed channel FFP both at the anode and cathode side. Both at the anode and cathode sides, a 200 μm-thick rubber sheet-made gasket (Kureha Elastomer Co. [41]) was used to cover the edges of the PTL.

In a PEM fuel cell or electrolyzer, the PTL is a key component that helps distribute reactants (toluene in this case) to the active electrode surface while also providing a conductive pathway for the generated electrons. As the reactants flow through the cathode side, there is a pressure drop that occurs because of the resistance of the porous material and the geometry of the flow fields. This pressure drop is not uniform across the PTL but rather varies depending on the location within the PTL. Specifically, the pressure tends to be highest at the inlet, where the reactants first enter, and decreases gradually as the reactants move further towards the exit. If the pressure drop is too high, the pumping consumption can increase and reduce the overall efficiency of the system. On the other hand, if the pressure drop is too low, it can lead to non-uniform reactant distribution and lower performance. Therefore, careful design and optimization of the PTL is important to ensure optimal performance of industrial scale electrolyzers. The thickness of PTL used in this research is very small 200 μm; the toluene flow through the PTL is dominated by viscous forces rather than inertia forces (low Reynolds number $\sim 10^{-3}$), thereby, it was assumed a uniform toluene flow distribution through PTL.

2.2. *Visualization and image processing*

A third-generation 3D Microscopic X-ray CT with a cone-shaped beam system (model TDM-1000H-II(2K) manufactured by Yamato Kagaku Co., Ltd. [42]) was used to visualize the inside of the operating electrolyzer cell. As shown in Fig. 4, the X-ray beam is irradiated from the source, and the transmitted image of the specimen is acquired at a small angle of 0.05°. In addition, by using a plane detector, multiple scan lines in the vertical direction are collected in a single scan, eliminating the need for vertical scanning, and enabling the acquisition of transmission images necessary for 3D reconstruction in a brief time. The separation between the sample and the X-Ray source was 100 mm (Fig. 2).

Table 1 summarizes the parameter settings for the X-ray CT system, which enable the best visualization results and are consistent with previous research [43]. Individual images (i.e.,

Please cite this article as: Reyna-Peña FI et al., In situ X-ray CT visualization of hydrogen bubbles inside the porous transport layer of a direct toluene electro-hydrogenation electrolyzer, International Journal of Hydrogen Energy, https://doi.org/10.1016/j.ijhydene.2023.08.132

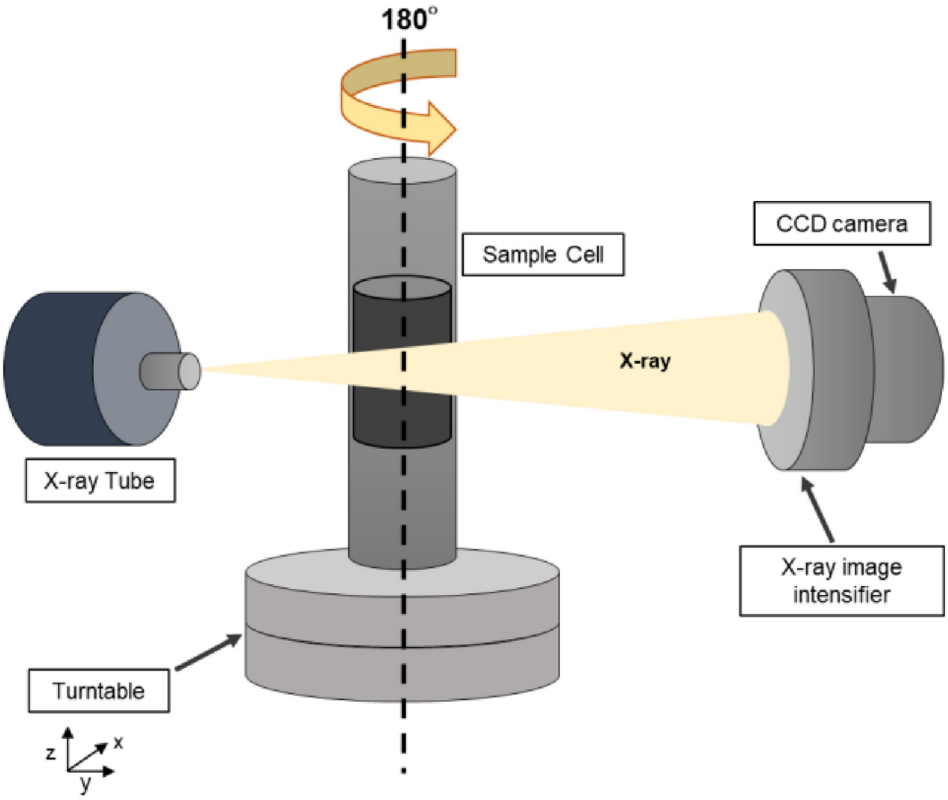

Fig. 4 – Schematic of visualization procedure of the X-Ray CT scan.

slices) were captured and gathered while the sample rotates continuously (180°, half rotation). Subsequently, all these slices are reconstructed resulting in a single stacked image. More slices lead to higher stacked image quality, but also longer scanning time. Considering these trade-offs, the scan time (half rotation) was set for 15 min.

Table 1 – Operating conditions set for the X-ray CT scan system.

Parameter	Value
Tube voltage	30 kV
Tube current	100 mA
Number of views	3600
Scanning time	15 min

The software ImageJ [44] and Dragonfly [45] were both used for the processing of the images obtained. As an example, Fig. 5 shows a cross-sectional view of the cathode's PTL (along the thickness direction) when the cell was operated at 30 mA/cm^2 for 30 min. Fig. 5 (a) depicts the raw image of a slice after applying automatic brightness and contrast correction. The gray level intensity ratio is an indicator used to analyze the results obtained in this work. It takes values between 0 and 100% so that higher values indicate lower X-ray absorption (i.e., darker zones shown in Fig. 5 (a)).

Even though hydrogen is more likely to exist in those darker regions of Fig. 5 (a) (because of its very low atomic mass, which leads to lower X-ray absorption), it is usually challenging to distinguish hydrogen bubbles not only from the other phases (e.g., toluene or MCH) but also from voids in the carbon fiber of

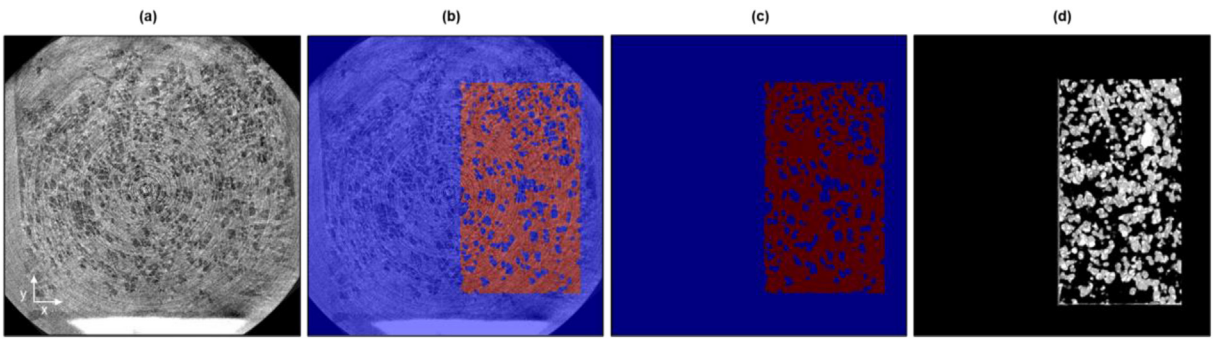

Fig. 5 – Image processing sequence for isolation of hydrogen bubbles. (a) Raw data, (b) preliminary (automatic) segmentation of a single slice, (c) final (refined) segmentation with removed background, (d) 3D hydrogen bubble distribution. Flow direction from bottom to top.

Please cite this article as: Reyna-Peña FI et al., In situ X-ray CT visualization of hydrogen bubbles inside the porous transport layer of a direct toluene electro-hydrogenation electrolyzer, International Journal of Hydrogen Energy, https://doi.org/10.1016/j.ijhydene.2023.08.132

the PTL. Therefore, the application of segmentation methods based on machine learning algorithms is required to localize hydrogen bubbles with a degree of accuracy.

Fig. 5 (b) depicts the preliminary segmentation result obtained for a single slice, and Fig. 5 (c) illustrates the final segmented slice after manual refinement and removing the layers corresponding to the cell background. Then, the image processing software applies the same segmentation criteria to the whole set of slices integrating the stacked image. Note that to enhance the accuracy and speed up the analysis process, the total active area captured in the visualizations (i.e., 1 cm^2) was cropped to focus on a smaller portion of 0.32 cm^2.

Finally, after binarizing the segmented slices, Fig. 5 (d) shows the 3D distribution of hydrogen bubbles inside the PTL. The "area fraction" technique [44] was used to measure the total hydrogen bubble fraction, which is the indicator used to evaluate the total percentage of hydrogen bubbles inside the entire PTL. Those pixels that correspond to hydrogen gas in the delimited active area in the binarized stacked images (i.e., white pixels) were automatically counted.

2.3. *Experimental conditions*

The distribution of hydrogen bubbles was visualized and analyzed under different operating conditions. Beyond the two FFP geometries considered (Fig. 3), experiments were conducted at the following current densities: 10, 20, and 30 mA/cm^2, while maintaining the X-ray CT operating conditions constant at 100 mA and 30 kV. On the other hand, experiments were conducted for 15-min and 30-min operations to discuss the effect of the operating time on the hydrogen bubble depletion and distribution.

The hydrogen and toluene flow rates were set at 2 mL/min and 0.1 mL/min, respectively, supplied with Smoothflow Pump Q Series [46]. A unit Biologic EC-LAB series SP-240 (Toyo Technical Co. Ltd. [47]) monitored the voltage, current and cell resistance (based on the EIS test) in every experiment. All subsequent tests were conducted before performing a visualization scan on the X-Ray CT for the different conditions each time.

Table 2 shows the parameters set for the tests performed prior to visualization experiments. Leak testing is crucial in fuel cells to ensure the safety and reliability of the system. Fuel cells typically use hydrogen gas, which is highly flammable and can be dangerous if leaked. A leak in the system can also compromise the performance of the fuel cell by causing a drop in pressure or flow rate, leading to reduced efficiency and potential damage to the cell components. The electrochemical impedance spectroscopy (EIS) test was conducted to check that the resistance was within the typical values. Additionally, the CT scan was purged for 45-min using nitrogen to ensure dry operating conditions.

Table 2 – Tests performed prior to visualization experiments.

Test	Aim/parameters
Leak Test	To verify that there were no outflows.
EIS	0.65 ~ 0.80 Ω. The values remained within these ranges for both FFP geometries.
CT Scan Dry	N_2 purge for 45 min.

3. Results and discussion

3.1. *Distribution of hydrogen bubbles*

Fig. 6 shows the gray level intensity ratio averaged along the PTL's thickness (i.e., z-direction) when the electrolyzer cell operates for 30-min operation, at various current densities

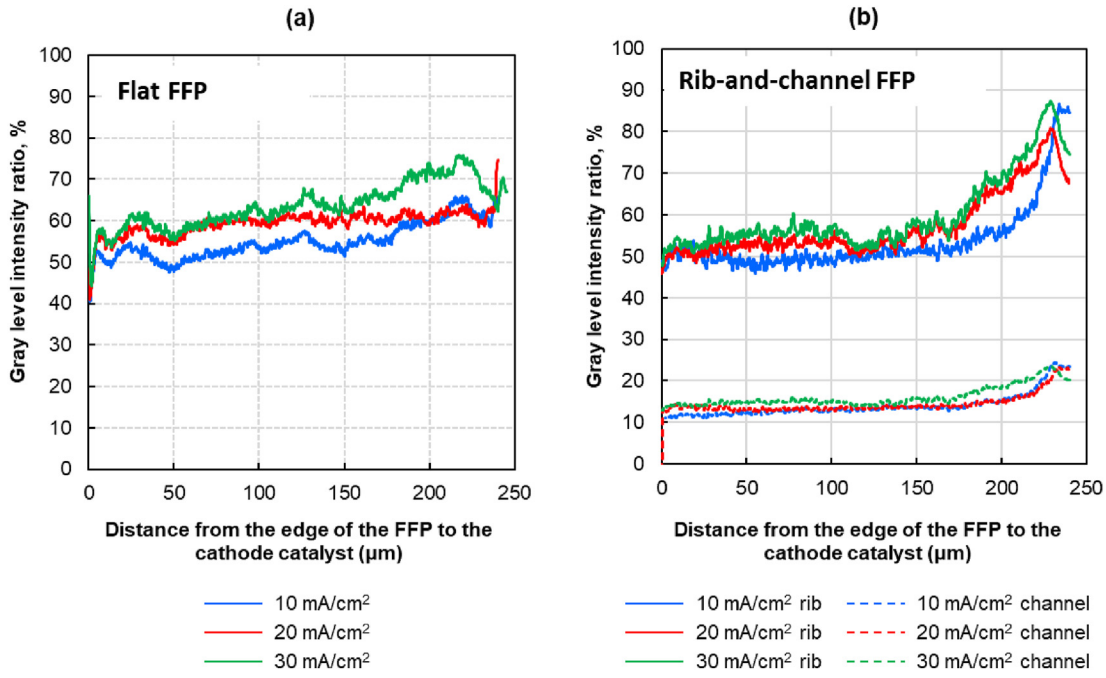

Fig. 6 – Distribution of hydrogen bubbles along the PTL's thickness (z-direction) at various current densities, for a 30-min operation using (a) flat and (b) rib-and-channel FFP.

Please cite this article as: Reyna-Peña FI et al., In situ X-ray CT visualization of hydrogen bubbles inside the porous transport layer of a direct toluene electro-hydrogenation electrolyzer, International Journal of Hydrogen Energy, https://doi.org/10.1016/j.ijhydene.2023.08.132

and using the different flow field geometries considered in this work.

For the case using a flat FFP depicted in Fig. 6 (a), the amount of hydrogen accumulated inside the cathode's PTL increases with the electric current. More electrons are supplied to the cathode reaction site as the electric current rises, thereby promoting the generation of hydrogen. Moreover, the concentration of hydrogen bubbles tends to increase along the PTL thickness (i.e., from the PTL/FFP interface towards the PTL/catalyst interface), so the highest accumulation of hydrogen was found near the cathode's reaction site.

As shown in Fig. 6 (b), the same trend observed for the flat FFP was also found in the PTL fraction beneath the ribs when using rib-and-channel FFP. Nevertheless, Fig. 6 (b) also indicates that the amount of hydrogen accumulated in the PTL fractions beneath channels is significantly lower than that under ribs. In addition, the number of bubbles is roughly constant along the PTL thickness. Channels provide a path to the generated hydrogen gas towards the cathode outlet, but ribs act as a physical barrier that hampers somehow the free movement of bubbles which may tend to accumulate.

To gain insight into the effect of the flow field on the bubble's distribution patterns, Fig. 7 shows the distribution of hydrogen in the PTL thickness direction (z-direction) obtained for the flat and rib-and-channel FFPs for 30-min operation and at 30 mA/cm^2. The darker zones observed in the raw stacked image given in Fig. 7 (a) indicate that the absence of structural elements in the flat FFP results in a distribution of bubbles that spread across the active area. Moreover, the post-processed image corresponding to the

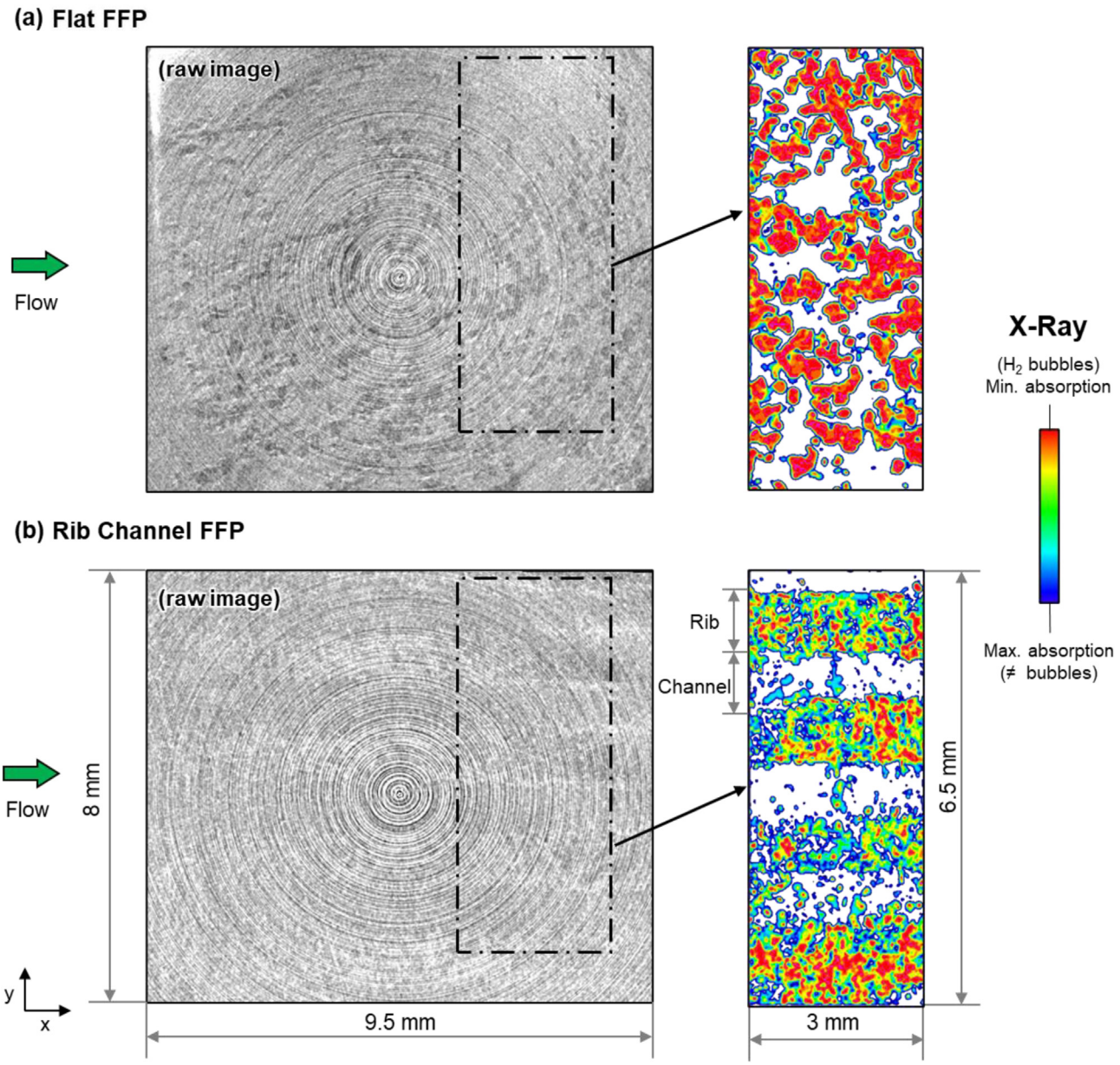

Fig. 7 – Hydrogen bubbles distribution in the thickness direction of the cathode PTL for a 30-min operation of the electrolyzer cell at a current density of 30 mA/cm^2, (a) Flat FFP, (b) Rib-and-channel FFP.

Please cite this article as: Reyna-Peña FI et al., In situ X-ray CT visualization of hydrogen bubbles inside the porous transport layer of a direct toluene electro-hydrogenation electrolyzer, International Journal of Hydrogen Energy, https://doi.org/10.1016/j.ijhydene.2023.08.132

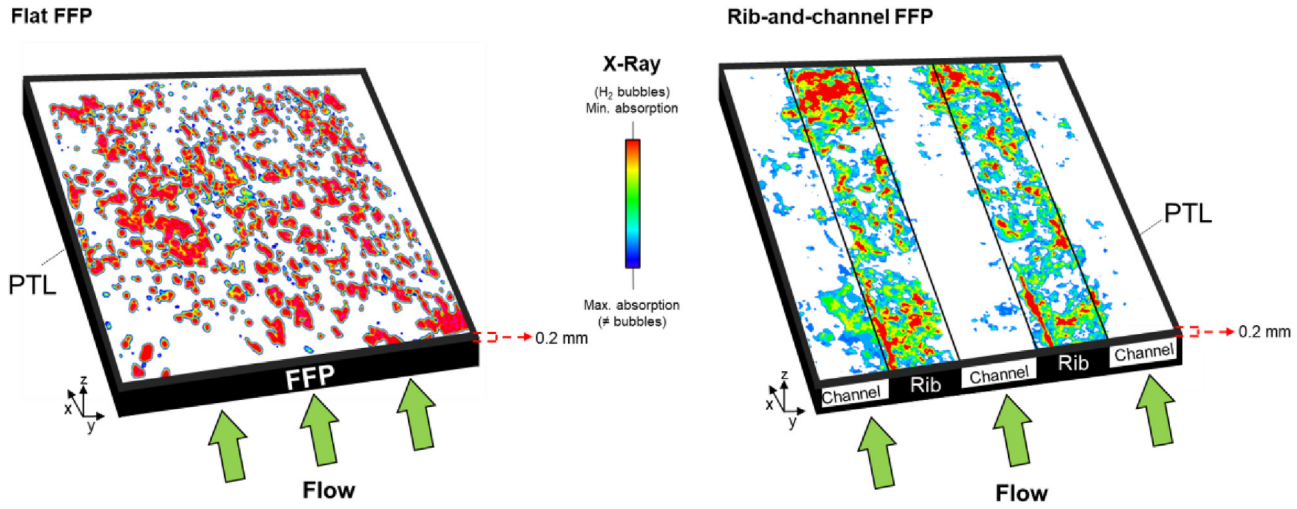

Fig. 8 – Hydrogen bubble distribution in the toluene flow direction at a current density of 30 mA/cm^2 for 30-min operation.

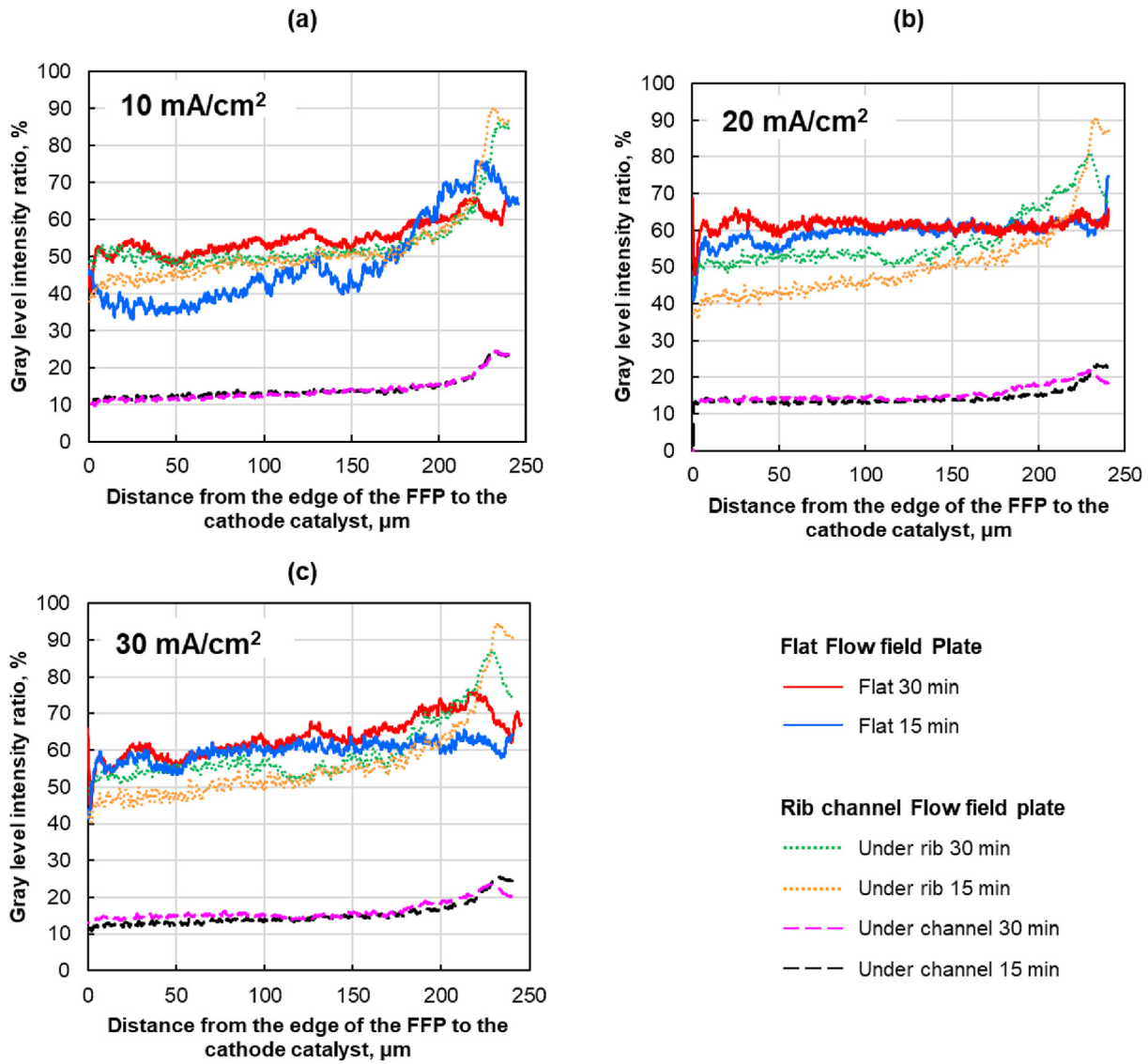

Fig. 9 – Average hydrogen bubble distribution inside the PTL thickness (z-direction) at various electric current densities and operating times.

Please cite this article as: Reyna-Peña FI et al., In situ X-ray CT visualization of hydrogen bubbles inside the porous transport layer of a direct toluene electro-hydrogenation electrolyzer, International Journal of Hydrogen Energy, https://doi.org/10.1016/j.ijhydene.2023.08.132

area delimited by the black-dotted line highlights the absence of local bubble concentration regions. In contrast, Fig. 7 (b) shows the more complex distribution pattern resulting from the use of a rib-and-channel FFP. This confirms the findings derived from Fig. 6.

The 3D view given in Fig. 8 shows the distribution of hydrogen bubbles through the toluene flow direction (i.e., x-direction). Because of the very low Reynolds number of toluene flowing through the PTL (Section 2.2), hydrogen bubbles tend to spread across the entire PTL surface when using a flat FFP. The minor concentration of hydrogen gas in the channels when using a rib-and-channel FFP was observed inside the entire PTL.

To analyze the effect of the operating time on the hydrogen bubble distribution, Fig. 9 depicts the local gray level intensity averaged through the PTL thickness after the cell was operated for 15 and 30-min. The effect of the operating time on the bubble accumulation beneath channels when using rib-and-channel FFPs is almost negligible. On the other hand, the general trend observed in the flat FFP and under the ribs of the rib-and-channel FFP is that the amount of hydrogen bubbles slightly increased with the operating time. Nonetheless, the differences observed between both operating times are not significant. Thus, operating the electrolyzer cell for 30-min will be enough to consider that the cell has reached a quasi-steady operating regime. The emission and production rate of bubbles was stabilized so that the amount of hydrogen that stayed in the PTL can be measured and analyzed.

The section below further discusses the effect of the operating time on the total hydrogen accumulated inside the entire PTL.

3.2. *Total bubble fraction inside the PTL*

Fig. 10 depicts the bubble fraction calculated for the entire active area (i.e., 1 cm^2) of the electrolyzer cell at various electric currents and operating times and from the binarized images.

At the lowest electric current case (i.e., 10 mA/cm^2), the bubble fraction using a flat FFP was 27.6% and 29.3% after 15 and 30-min operation, respectively; the rib-and-channel FFP had a bubble fraction of approximately 20.6% and 23.1% for 15 and 30-min operation, respectively. At the highest current density operation (30 mA/cm^2), the flat FFP had a bubble fraction of approximately 34.9% and 39.8% after the cell operated for 15 and 30-min, respectively; the rib-and-channel FFP had a bubble fraction of approximately 21.5% after 15 min and 27.4% after 30-min operation.

The analysis of the bubble fraction percentage highlights that the total amount of hydrogen gas may be reduced by using the rib-and-channel FFP geometry. Nevertheless, the average distance of the toluene flow toward the catalyst layer is higher for the rib-and-channel geometry than in the case of a flat FFP. The absence of channels provides toluene with a shorter and direct path to the PTL across its entire surface, thereby promoting the toluene supply to the reaction site inside the catalyst layer, which may be positive in terms of the electrochemical performance.

The trade-offs between the two FFP geometries highlight the significance of optimizing the design based on the intended application and performance requirements of the electrochemical device.

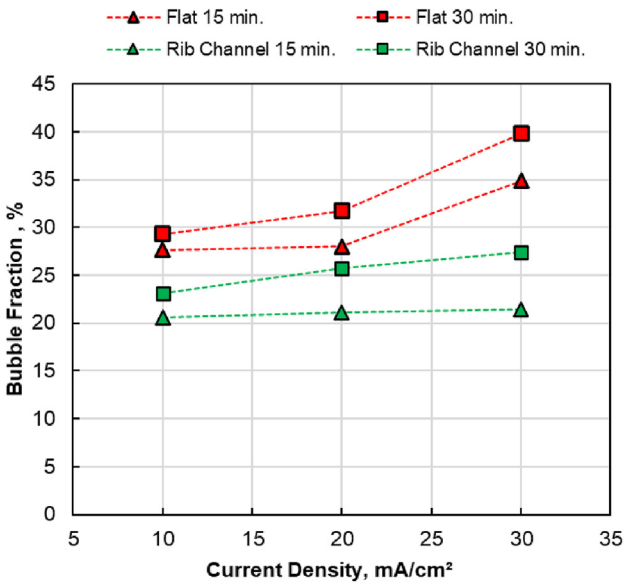

Fig. 10 – Bubble fraction in the PTL at 10, 20 and 30 mA/cm^2 for 15 and 30-min operation.

4. Conclusion

This paper presented the visualization using Microscopic X-ray technology of the bubble distribution and depletion, for the first time, inside the porous transport layer of an operating direct toluene electro-hydrogenation electrolyzer.

Hydrogen bubbles are transported from the FFP interface toward the cathode catalyst layer. As the electric current increased, more hydrogen bubbles were observed. Longer operating times tend to increase the total number of hydrogen bubbles along the PTL. The visualizations showed that the distribution of hydrogen bubbles spread across the whole active area when using flat FFPs. As for rib-and-channel FFPs, hydrogen bubbles are mostly concentrated under the ribs, and channels enhance the bubble removal from the PTL towards the cathode outlet, thereby reducing the overall number of bubbles. Rib-and-channel FFPs allow reducing the pressure drop concerning flat geometries, leading to lower pumping energy consumption. This translates to cost-effective operations and enhanced energy efficiency. However, channels introduce a greater distance between the toluene supplied and the cathode catalyst layer, which may reduce the current efficiency. In contrast, flat FFPs without channels provide a direct path for toluene to reach the reaction site, which can improve the conversion rate of toluene to methylcyclohexane. Flat geometries offer greater space efficiency, which makes them attractive for applications where space is limited.

The use of imaging techniques can provide valuable insights into the behavior of hydrogen bubbles within electrochemical devices. The results of this visualization study can serve as a reference for optimizing the mass transfer in direct toluene hydrogenation based on PEM-type electrolyzers technology and improve their future designs.

Please cite this article as: Reyna-Peña FI et al., In situ X-ray CT visualization of hydrogen bubbles inside the porous transport layer of a direct toluene electro-hydrogenation electrolyzer, International Journal of Hydrogen Energy, https://doi.org/10.1016/j.ijhydene.2023.08.132

Declaration of competing interest

The authors declare that they have no known competing financial interests or personal relationships that could have appeared to influence the work reported in this paper.

Acknowledgments

This study was based on results obtained from the Development of Fundamental Technology for Advancement of Water Electrolysis Hydrogen Production in Advancement of Hydrogen Technologies and Utilization Project (P14021) commissioned by the New Energy and Industrial Technology Development Organization (NEDO). Fátima Isabella Reyna-Peña acknowledges a predoctoral scholarship granted by the Ministry of Education, Culture, Sports, Science and Technology (MEXT) of Japan. Antonio Atienza-Márquez acknowledges the Ministerio de Universidades of Spain and the Recovery, Transformation and Resilience Plan for financially supporting the postdoctoral contract 2021URV-MS-01. The authors would like to thank Anika I. Raschun for their contribution to the design of the images used in this paper.

REFERENCES

[1] International Renewable Energy Agency (IRENA). World energy transitions outlook 2022: 1.5°C pathway. 2022.
[2] Atienza-Márquez A, Bruno JC, Coronas A. Regasification of liquefied natural gas in satellite terminals: techno-economic potential of cold recovery for boosting the efficiency of refrigerated facilities. Energy Convers Manag 2021;248:114783. https://doi.org/10.1016/j.enconman.2021.114783.
[3] International Energy Agency (IEA). The global energy crisis pushed fossil fuel consumption subsidies to an all-time high in. 2022. n.d, https://www.iea.org/commentaries/the-global-energy-crisis-pushed-fossil-fuel-consumption-subsidies-to-an-all-time-high-in-2022. [Accessed 17 March 2023].
[4] International Energy Agency (IEA). CO_2 emissions in 2022. 2022.
[5] Hassan Q, Abdulateef AM, Hafedh SA, Al-samari A, Abdulateef J, Sameen AZ, et al. Renewable energy-to-green hydrogen: a review of main resources routes, processes, and evaluation. Int J Hydrogen Energy 2023. https://doi.org/10.1016/j.ijhydene.2023.01.175.
[6] Niermann M, Beckendorff A, Kaltschmitt M, Bonhoff K. Liquid organic hydrogen carrier (LOHC) – assessment based on chemical and economic properties. Int J Hydrogen Energy 2019;44:6631–54. https://doi.org/10.1016/j.ijhydene.2019.01.199.
[7] Hassan IA, Ramadan HS, Saleh MA, Hissel D. Hydrogen storage technologies for stationary and mobile applications: review, analysis, and perspectives. Renew Sustain Energy Rev 2021;149. https://doi.org/10.1016/J.RSER.2021.111311.
[8] Aakko-Saksa PT, Cook C, Kiviaho J, Repo T. Liquid organic hydrogen carriers for transportation and storing of renewable energy – review and discussion. J Power Sources 2018;396:803–23. https://doi.org/10.1016/j.jpowsour.2018.04.011.
[9] Abdin Z, Tang C, Liu Y, Catchpole K. Large-scale stationary hydrogen storage via liquid organic hydrogen carriers n.d. https://doi.org/10.1016/j.isci.
[10] Rao P, Yoon M. Potential liquid-organic hydrogen carrier (LOHC) systems: a review on recent progress. Energies 2020;13:6040. https://doi.org/10.3390/en13226040.
[11] Zhang C, Song P, Zhang Y, Xiao L, Hou J, Wang X. Technical and cost analysis of imported hydrogen based on MCH-TOL hydrogen storage technology. Int J Hydrogen Energy 2022;47:27717–32. https://doi.org/10.1016/j.ijhydene.2022.06.113.
[12] Markiewicz M, Zhang Y-Q, Empl MT, Lykaki M, Thöming J, Steinberg P, et al. Hazard assessment of quinaldine-, alkylcarbazole-, benzene- and toluene-based liquid organic hydrogen carrier (LOHCs) systems. Energy Environ Sci 2019;12:366–83. https://doi.org/10.1039/C8EE01696H.
[13] Wijayanta AT, Oda T, Purnomo CW, Kashiwagi T, Aziz M. Liquid hydrogen, methylcyclohexane, and ammonia as potential hydrogen storage: comparison review. Int J Hydrogen Energy 2019;44:15026–44. https://doi.org/10.1016/j.ijhydene.2019.04.112.
[14] Lee JS, Cherif A, Yoon HJ, Seo SK, Bae JE, Shin HJ, et al. Large-scale overseas transportation of hydrogen: comparative techno-economic and environmental investigation. Renew Sustain Energy Rev 2022;165. https://doi.org/10.1016/J.RSER.2022.112556.
[15] Zahid AH, Amin N, Nisar F, Saghir S. Analysis of MTH-System (Methylcyclohexane-Toluene-Hydrogen-System) for hydrogen production as fuel for power plants. Int J Hydrogen Energy 2020;45:32234–42. https://doi.org/10.1016/j.ijhydene.2020.08.248.
[16] Shigemasa K, Atienza-Márquez A, Inoue K, Jang S, Peña FIR, Araki T, et al. Visualization of dragged water and generated hydrogen bubbles in a direct toluene electro-hydrogenation electrolyzer. J Power Sources 2023;554:232304. https://doi.org/10.1016/j.jpowsour.2022.232304.
[17] Nagasawa K, Sawaguchi Y, Kato A, Nishiki Y, Mitsushima S. Chemical-hydrogenation functionalized flow-field in toluene direct electro-hydrogenation electrolyzer for energy-carrier synthesis system. Electrochemistry 2018;86:339–44. https://doi.org/10.5796/electrochemistry.18-00055.
[18] Oi S, Nagasawa K, Takamura T, Misu Y, Matsuoka K, Mitsushima S. Control of transport water in direct toluene electro-hydrogenation electrolyzer. ECS Meeting Abstracts 2021;MA2021–02:1737. https://doi.org/10.1149/MA2021-02581737mtgabs.
[19] Nagasawa K, Sugita Y, Atienza-Márquez A, Kuroda Y, Mitsushima S. Effect of the cathode catalyst loading on mass transfer in toluene direct electrohydrogenation. J Electroanal Chem 2023:117431. https://doi.org/10.1016/j.jelechem.2023.117431.
[20] Nagasawa K, Kato A, Nishiki Y, Matsumura Y, Atobe M, Mitsushima S. The effect of flow-field structure in toluene hydrogenation electrolyzer for energy carrier synthesis system. Electrochim Acta 2017;246:459–65. https://doi.org/10.1016/j.electacta.2017.06.081.
[21] Nagasawa K, Sawaguchi Y, Kato A, Nishiki Y, Mitsushima S. Rate-determining factor of the performance for toluene electrohydrogenation electrolyzer. Electrocatalysis 2017;8:164–9. https://doi.org/10.1007/s12678-017-0351-4.
[22] Nagasawa K, Tanimoto K, Koike J, Ikegami K, Mitsushima S. Toluene permeation through solid polymer electrolyte during toluene direct electro-hydrogenation for energy carrier synthesis. J Power Sources 2019;439:227070. https://doi.org/10.1016/j.jpowsour.2019.227070.
[23] Mitsushima S, Takakuwa Y, Nagasawa K, Sawaguchi Y, Kohno Y, Matsuzawa K, et al. Membrane electrolysis of toluene hydrogenation with water decomposition for energy

carrier synthesis. Electrocatalysis 2016;7:127–31. https://doi.org/10.1007/s12678-015-0289-3.
[24] Xin S, LiJun X, Di Z, Bing H, Mi LuXiang M. Electrochemical performance study of proton exchange membrane electrolyzer considering the effect of bubble coverage. Int J Hydrogen Energy 2023;70:27079–94. https://doi.org/10.1016/j.ijhydene.2023.03.247.
[25] Bazylak A. Liquid water visualization in PEM fuel cells: a review. Int J Hydrogen Energy 2009;34(9):3845–57. https://doi.org/10.1016/j.ijhydene.2009.02.084.
[26] Lee SJ, Lim N-Y, Kim S, Park G-G, Kim C-S. X-ray imaging of water distribution in a polymer electrolyte fuel cell. J Power Sources 2008;185(2):867–70. https://doi.org/10.1016/j.jpowsour.2008.08.101.
[27] Sasabe T, Tsushima S, Hirai S. In-situ visualization of liquid water in an operating PEMFC by soft X-ray radiography. Int J Hydrogen Energy 2010;35(20):11119–28. https://doi.org/10.1016/j.ijhydene.2010.06.050.
[28] Leonard E, Shum AD, Normile S, Sabarirajan DC, Yared DG, Xiao X, Zenyuk IV. Operando X-ray tomography and sub-second radiography for characterizing transport in polymer electrolyte membrane electrolyzer. Electrochim Acta 2018;276:424–33. https://doi.org/10.1016/j.electacta.2018.04.144.
[29] Satjaritanun P, O'Brien M, Kulkarni D, Shimpalee S, Capuano C, Ayers KE, Danilovic N, Parkinson DY, Zenyuk IV. Observation of preferential pathways for oxygen removal through porous transport layers of polymer electrolyte water electrolyzers. iScience 2020;23(12):101783. https://doi.org/10.1016/j.isci.2020.101783.
[30] Markötter H, Alink R, Haußmann J, Dittmann K, Arlt T, Wieder F, Tötzke C, Klages M, Reiter C, Riesemeier H, Scholta J, Gerteisen D, Banhart J, Manke I. Visualization of the water distribution in perforated gas diffusion layers by means of synchrotron X-ray radiography. Int J Hydrogen Energy 2012;37(9):7757–61. https://doi.org/10.1016/j.ijhydene.2012.01.141.
[31] Kato A, Kato S, Yamaguchi S, Suzuki T, Nagai Y. Dependence of vapor and liquid water removal on cross-flow in polymer electrolyte fuel cell investigated by operando synchrotron X-ray radiography. Int J Hydrogen Energy 2023. https://doi.org/10.1016/j.ijhydene.2023.06.239.
[32] Banerjee R, Ge N, Han C, Lee J, George MG, Liu H, Muirhead D, Shrestha P, Bazylak A. Identifying in operando changes in membrane hydration in polymer electrolyte membrane fuel cells using synchrotron X-ray radiography. Int J Hydrogen Energy 2018;43(20):9757–69. https://doi.org/10.1016/j.ijhydene.2018.03.224.
[33] Ercelik M, Ismail MS, Hughes KJ, Ingham DB, Ma L, Pourkashanian M. X-ray CT-based numerical investigation of nickel foam-based GDLs under compression. Int J Hydrogen Energy 2023. https://doi.org/10.1016/j.ijhydene.2023.07.001.
[34] James JP, Choi H-W, Pharoah JG. X-ray computed tomography reconstruction and analysis of polymer electrolyte membrane fuel cell porous transport layers. Int J Hydrogen Energy 2012;37(23):18216–30. https://doi.org/10.1016/j.ijhydene.2012.08.077.
[35] Spiegel C. Designing and building fuel cells. New York: McGraw-Hill; 2007.
[36] Limjeerajarus Nuttapol, Charoen-amornkitt Patcharawat. Effect of different flow field designs and number of channels on performance of a small PEFC. Int J Hydrogen Energy 2015;40(22):7144–58. https://doi.org/10.1016/j.ijhydene.2015.04.007.
[37] Yoon Young-Gi, Lee Won Yong, Park Gu-Gon, Yang T-H, Kim Chang-Soo. Effects of channel and rib widths of flow field plates on the performance of a PEMFC. Int J Hydrogen Energy 2005;30(12):1363–6. https://doi.org/10.1016/j.ijhydene.2005.04.008.
[38] G347B Tokai Carbon Co, (Accessed: 6 June 2023 https://www.tokaicarbon.co.jp/en/products/fine_carbon/pdf/Isotropic_graphite.pdf.
[39] GORE-SELECT®, https://www.gore.com/(Accessed: 6 June 2023).
[40] SGL39BC and BB, https://www.eiwa-net.co.jp/index.php (Accessed: 6 June 2023).
[41] EB62J5S, https://biz.maxell.com/en/elastomer/(Accessed: 6 June 2023).
[42] 3D X-Ray Microscopic CT Scanner TDM-1000 https://www.yamato-scientific.com/(Accessed: 6 June 2023).
[43] Shigemasa K, Sato H, Otsuki Y, Kurosu M, Araki T. Investigating the vapour transport phenomena inside the cathode gas diffusion layer media by controlling local temperature gradient inside an operating proton exchange membrane fuel cell. Electrochim Acta 2021;365:137383. https://doi.org/10.1016/j.electacta.2020.137383.
[44] Wayne Rasband, ImageJ User Guide IJ1.46r, https://imagej.nih.gov/ij/docs/guide/user-guide.pdf.
[45] Maxnet Co., Ltd. Dragonfly https://www.maxnt.co.jp/products/Dragonfly.html.
[46] Tacmina, https://www.tacmina.com/(Accessed: 6 June 2023).
[47] Biologic, https://www.biologic.net/(Accessed: 6 June 2023).

Please cite this article as: Reyna-Peña FI et al., In situ X-ray CT visualization of hydrogen bubbles inside the porous transport layer of a direct toluene electro-hydrogenation electrolyzer, International Journal of Hydrogen Energy, https://doi.org/10.1016/j.ijhydene.2023.08.132